Available online at www.sciencedirect.com
SCIENCE DIRECT®
Journal of Catalysis 223 (2004) 74–85
JOURNAL OF CATALYSIS
www.elsevier.com/locate/jcat

An exploration of activity loss during hydrodechlorination and hydrodebromination over Ni/SiO_2

K.V. Murthy,[a] Patricia M. Patterson,[b] Gary Jacobs,[b] Burtron H. Davis,[b] and Mark A. Keane [a,*]

[a] *Department of Chemical and Materials Engineering, University of Kentucky, Lexington, KY 40511, USA*
[b] *Center for Applied Energy Research, University of Kentucky, Lexington, KY 40506, USA*

Received 18 September 2003; revised 24 December 2003; accepted 7 January 2004

Abstract

The gas-phase catalytic hydrodechlorination (HDC) of 1,3-dichlorobenzene (1,3-DCB) and hydrodebromination (HDB) of 1,3-dibromobenzene (1,3-DBB) have been studied ($T = 573$ K) over Ni/SiO_2. The catalyst was 100% selective in terms of hydrodehalogenation where HDC far exceeded HDB, an effect that is attributed to substituent inductive effects. Catalytic activity declined with time on stream with a concomitant increase in partial dehalogenation (to the mono-haloarene). A precontact of the catalyst with the haloarene resulted in a complete loss of any hydrogenation activity. The pre- and postreaction catalyst samples have been characterized by TPR, TEM, H_2 chemisorption, TPD, XRD, and XANES/EXAFS. Appreciable Ni particle growth during catalysis (particularly HDB) has been observed with Ni particle faceting, which is attributed to a halide-induced metal agglomeration/reconstruction; there was no evidence of any bulk nickel halide formation. The possible effect of nickel sintering on hydrodehalogenation was considered by inducing particle growth by thermal means where the resultant sintering did not result in any significant loss of catalytic activity. Catalyst deactivation is linked to a restructuring of the Ni sites during reaction that serves to disrupt H_2 chemisorption/desorption dynamics: the used samples exhibit a lower H_2 uptake with weaker surface interactions.

Keywords: Catalytic hydrodehalogenation; Dichlorobenzene; Dibromobenzene; Nickel/silica; TPR; TPD; XRD; XANES/EXAFS

1. Introduction

Halogenated organic compounds find commercial use in the synthesis of deodorants, dyes, solvents, pesticides, and as intermediates in dielectric fluids [1–3] where any associated halogen-containing waste streams are typically classified as hazardous/nonbiodegradable with adverse ecologic and public health impacts [4–6]. Many haloarenes, the topic of this report, now appear on the USEPA list of priority pollutants, targeted in terms of emission control [7]. Incineration is the preferred means of treatment [8,9], albeit halogenated waste is characterized by low Btu values while dioxin/furan formation can result from incomplete combustion [10,11]. Given the increasingly stringent environmental regulations, there is now a concerted move to benign alternatives and catalytic hydrodehalogenation is emerging as one of the most promising and progressive low energy/nondestructive technologies [12]. Hydrodehalogenation, the hydrogen cleavage of C–X (carbon–halogen) bonds, yields the respective hydrogen halide and recoverable chemical feedstock with no dioxin formation. In thermal hydrogenolysis, the halogen substituents are displaced by H at a faster rate than arene ring degradation [13]; the use of supported metal catalysts significantly lowers the reaction energetics [12].

Catalyst deactivation is a common feature of the hydrodechlorination (HDC) of both aliphatic and aromatic reactants over an array of supported metal catalysts, an effect that has been attributed to either carbon deposition/occlusion of the active metal sites and/or surface poisoning by HCl and/or metal sintering [14–23] but no conclusive deactivation mechanism has yet emerged. Moreover, the nature of reactive adsorbed species and catalytically active sites is still open to question but it is generally accepted that hydrodehalogenation, in common with most hydrogenolysis reactions, is strongly influenced by the electronic structure of the

* Corresponding author.
E-mail address: makeane@engr.uky.edu (M.A. Keane).

0021-9517/$ – see front matter
doi:10.1016/j.jcat.2004.01.004

metal sites [24] where the nature of the support can influence catalyst stability [25,26]. Focusing on supported Ni, the subject of this study, there are a number of reports that deal, to varying degrees of detail in terms of kinetic and catalyst structural data, with the gas-phase HDC of chlorobenzene [16,27–36]. The removal of multiple chlorine atoms from an aromatic host has also been studied to a lesser extent [27,33, 34,37–39] while hydrodebromination (HDB) reactions have received scant attention in the literature [22,28,40–42]. In flagging some specific publications relating to catalyst deactivation that are pertinent to our study, we can point to the HDC of 1,3-dichloropropane over Ni/SiO_2–Al_2O_3 and Ni–Mo/γ-Al_2O_3 (at 698 K) [43] where the former catalyst exhibited significant activity with no sign of any deactivation over a period of 13 h on stream while the Ni–Mo system was subject to appreciable activity loss. The HDC of 1,2-dichloropropane (at 573 K) over Ni/SiO_2 was found to be sensitive to Ni loading (5–40% w/w Ni), where a 10% w/w Ni content (Ni particle size = 25 nm) showed the highest activity but a greater susceptibility to deactivation than was observed for larger (51 nm at 20% w/w Ni) particles [44]; activity loss was attributed to $NiCl_2$ formation/metal sintering. In the gas-phase HDC of polychlorinated hydrocarbons over sulfided Ni-Mo/γ-Al_2O_3 (100 bar, 623 K) a decrease in activity over prolonged (> 58 h) reaction times has been linked to a loss of surface area (from 178 to 124 $m^2\,g^{-1}$) [45]. Morato et al. [46], in studying the hydrodehalogenation of chlorofluromethane (523–563 K) over bulk and carbon-supported Ni have reported a higher activity for unsupported Ni that they ascribed to a preferential octahedral (200–400 nm) Ni particle structure. Unsupported Ni also suffered deactivation during the HDC of 1,2-dichlorobenzene [31] where larger octahedral crystallites ($\geqslant 200$ nm) again delivered a higher specific activity. The level of 1,2,4-trichlorobenzene HDC over Ni/Mg/Al hydrotalcite (523 K) [47,48] was both enhanced and stabilized with an increase in Mg content but a loss of activity was still observed. In contrast, Lingaiah et al. [36] did not record any decline in chlorobenzene (523–673 K) HDC over a Ni/C composite catalyst.

The results presented in this report represent an extension of previous studies [42,49–52] that demonstrated the viability of nanoscale supported Ni to detoxify concentrated halogenated aromatic gas streams where activity/selectivity and catalyst stability were very much dependent on metal/support interactions with a high degree of structure sensitivity. In this paper we consider the dehalogenation of 1,3-dichlorobenzene (1,3-DCB) and 1,3-dibromobenzene (1,3-DBB) as model reactants over Ni/SiO_2, addressing the nature of haloarene reactivity and the changes that are wrought to the catalyst structure: we provide characterization (TEM, TPR, H_2 chemisorption/TPD, XRD, and XANES/EXAFS) results for the catalyst before and after use.

2. Experimental

2.1. Catalyst preparation and activation

A ca. 7% w/w (determined by ICP-OES, Vista-PRO, Varian Inc.) Ni on SiO_2 (Aldrich, surface area = 205 $m^2\,g^{-1}$) precursor was prepared by standard impregnation, where a 2-butanol nickel nitrate solution was added dropwise to the substrate at 353 K with constant agitation (600 rpm). The catalyst precursor was washed with 2-butanol and dried at 383 K, sieved in the 500- to 100-μm mesh range and reduced directly in a 60 $cm^3\,min^{-1}$ stream of ultrapure dry H_2 heated at 10 $K\,min^{-1}$ to 723 or 873 (±1) K, which was maintained for 12 h. A physical mixture (thorough mixing was ensured) of $NiO + SiO_2$ was also employed for comparative purposes, where the Ni content in the mixture = 7% w/w Ni. After reduction (as above) or after catalysis, the catalyst was flushed for 1 h in a stream of He, cooled (in He) to room temperature, and passivated in (40 $cm^3\,min^{-1}$) 5% v/v O_2/He for subsequent off-line characterization analysis.

2.2. BET/TPR/H_2 chemisorption/TPD analysis

The BET surface area, temperature-programmed reduction (TPR), hydrogen chemisorption, and temperature-programmed desorption (TPD) associated with the freshly activated and spent (both passivated) samples were determined using the commercial CHEM-BET 3000 (Quantachrome) unit: the unreduced Ni/SiO_2 precursor and $NiO + SiO_2$ physical mixture were also analyzed. The total surface area was recorded in a 30% v/v N_2/He flow; pure N_2 (99.9%) served as the internal standard. After outgas at 523 K for 30 min, at least two cycles of nitrogen adsorption–desorption in the flow mode were employed using the standard single-point BET method. Directly after BET measurement, the samples (ca. 0.2 g fresh or spent) were heated in a U-shaped Pyrex glass cell (10 cm × 3.76 mm i.d.) in 20 $cm^3\,min^{-1}$ (Brooks mass-flow controller) 5% v/v H_2/N_2 to 723 (or 873) K at 10 $K\,min^{-1}$ and the effluent gas was passed through a liquid N_2 trap; H_2 consumption was monitored by a thermal conductivity detector (TCD) with data acquisition/manipulation using the TPR Win software. The samples were maintained at 723 K for 12 h in a constant flow of H_2, swept with 20 $cm^3\,min^{-1}$ dry N_2 for 1 h at 723 K, cooled to room temperature, and subjected to H_2 chemisorption using a pulse (50–100 μl) titration procedure. The sample was thoroughly flushed with pure N_2 (20 $cm^3\,min^{-1}$) for 30 min to remove weakly bound hydrogen. Temperature-programmed desorption was conducted in the N_2 flow at 50 $K\,min^{-1}$ to 723 K with an isothermal hold of 15 min. The BET surface areas recorded after TPR/H_2 chemisorption/TPD were unchanged: BET surface area and hydrogen uptake values were reproducible to within ±5%; the values quoted in this paper are the mean.

2.3. TG/MS analysis

Temperature-programmed treatment of the reduced/passivated unused/used catalysts was also undertaken using a Seiko Instruments Inc. TG/DTA 320 simultaneous thermogravimetric/differential thermal analyzer coupled to a MICROMASS PC residual gas analyzer. A known quantity of catalyst (ca. 18 mg) was placed in a Pt sample pan and heated from 298 to 1173 K at 5 K min^{-1} in a reducing atmosphere (100 cm^3 min^{-1} He + 20 cm^3 min^{-1} H_2), monitoring the effluent gas over the mass range 10–100.

2.4. TEM analysis

High-resolution transmission electron microscopy (HRTEM) analysis was carried out using a Philips CM200 FEGTEM microscope operated at an accelerating voltage of 200 kV. The specimens were prepared by ultrasonic dispersion in 2-butanol, evaporating a drop of the resultant suspension onto a holey carbon support grid. The Ni particle-size distribution profiles presented in this report are based on a measurement of over 400 individual particles. The average Ni particle diameter (d_{av}) was calculated from

$$d_{av} = \frac{\sum_i n_i d_i}{\sum_i n_i},$$

where n_i is the number of particles of diameter d_i and $\sum_i n_i > 400$.

2.5. XRD analysis

Powder X-ray diffractograms (XRD) were recorded with a Philips X'Pert instrument using nickel-filtered Cu-K_α radiation. The samples were mounted in a low background sample holder and scanned at a rate of 0.02° per step over the $20° \leqslant 2\theta \leqslant 85°$ range with a scan time of 5 s $step^{-1}$. The diffractograms were compared with the JCPDS-ICDD [53] references for identification purposes.

2.6. EXAFS/XANES analysis

X-ray absorption (XAS) spectra at the Ni K edge (8.333 keV) of reference and catalyst samples were recorded in the energy range 8.1 to 9.3 keV using synchrotron radiation at the National Synchrotron Light Source (NSLS) at Brookhaven National Laboratory (BNL), beamline X18b. The X-ray ring at the NSLS has a flux of 1×10^{10} photons s^{-1} at 100 mA and 2.5 GeV. The X-ray monochromator at beamline X18b is equipped with a Si(111) channel-cut monochromator and has an energy range capability of 5.8 to 40 keV. The crystal was detuned slightly to prevent glitches due to harmonics. Extended X-ray absorption fine structure (EXAFS) spectra were recorded at 77 K to minimize contribution from the dynamic Debye–Waller factor and XANES spectra were recorded at ambient temperature. In all cases the spectra were measured in transmission mode. Ionization chambers were used for the detection of primary (I_0, 100% N_2) and transmitted (I_t, 75% N_2, balance Ar) beam intensities. The samples were diluted with BN (0.1 g catalyst + 0.3 g BN), pressed into self-supporting wafers, and mounted in copper blocks (to facilitate heat conduction). Reference materials used for X-ray absorption near-edge spectroscopy (XANES) measurements included Ni foil, NiO, $NiCl_2$, and $NiBr_2$.

Standard data reduction was carried out using the WinXAS program [54,55] with preedge background removal and normalization by division of the height of the absorption edge. XANES spectra and corresponding derivative spectra were compared after normalization. For EXAFS, χ data were obtained by considering the single scattering region from 50 eV after the edge jump. Appropriate splines based on the Nyquist criteria were utilized to remove the post-edge background to avoid the inclusion of excessive nodes that could destroy real oscillations. Conversion to k space was then conducted and k weights of zero and 3 were used, the former to allow viewing of chemical changes associated with low Z backscatterers and the latter carried out so that examination of the changes in Ni–Ni coordination of the catalyst metal clusters could be ascertained after conversion to R space. The k space results were transformed to R space to obtain the radial distribution functions. Isolating the first Ni–Ni coordination shell followed by an inverse Fourier transform was performed to obtain quantitative information on the degree of Ni–Ni coordination. Fitting of the spectra was carried out in k space using FEFFIT [56]; a k range from 4 to 15 $Å^{-1}$ was employed. Theoretical EXAFS were generated using FEFF [57] for model nickel and NiO using parameters generated by the Atoms [58] program. In order to use coordination number as a fitting parameter for Ni–Ni metal coordination, an amplitude reduction factor, S_0^2, was obtained by analyzing the nickel foil, employing a coordination number of 12 for the first shell of fcc Ni: S_0^2 was then fixed at 0.8652 ± 0.018. Other fitting parameters used by FEFFIT included the overall E_0 shift (e_0) applied to each path, delta r, to account for lattice expansion and σ^2, based on a correlated Debye model, used to approximate the mean square disorder in each path length. XANES spectra for the Ni foil, reduced/passivated Ni/SiO_2, and used reduced/passivated Ni/SiO_2 were isolated from the corresponding EXAFS scans following background subtraction and normalization of the edge jump.

2.7. Catalysis procedure

Reactions were carried out under atmospheric pressure, in situ immediately after activation, in a fixed-bed glass reactor (i.d. = 15 mm) at 573 K. The catalytic reactor has been described previously in detail elsewhere [29,50] but some features, pertinent to this study, are given below. The 1,3-DCB and 1,3-DBB reactants (Aldrich, 99.9%) were fed by means of a microprocessor-controlled infusion pump (Model 100, kd Scientific) via a glass/Teflon air-tight sy-

ringe and a Teflon line to the reactor in a stream of ultrapure H_2 (60 $cm^3\,min^{-1}$): the flow rate was monitored using a Humonics 520 digital flow meter. Catalytic activity and selectivity were assessed at a fixed inlet molar halogen/Ni ratio = 16.7 h^{-1}, where the LHSV (0.4 h^{-1}) and GHSV (1200 h^{-1}) were kept constant. The hydrogenation of benzene (Aldrich, 99.9%) was studied immediately before and after the hydrodehalogenation reactions at 393 K: molar benzene/Ni ratio = 13.2 h^{-1}. The reaction products were collected in a liquid N_2 trap over a period of 8 h and analyzed by capillary GC as described elsewhere [52]. Catalyst regeneration was attempted where the haloarene feed (after 8 h on-stream) was cut and the catalyst swept with dry H_2 at 60 $cm^3\,min^{-1}$ for 1 h at 573 K with subsequent ramping (10 $K\,min^{-1}$) and an isothermal hold at 723 K for 16 h. Qualitative analyses for the presence of Cl_2 or Br_2 gas were negative in every instance, confirming that hydrogenolytic cleavage yields HCl or HBr as the only inorganic product [29]. Catalytic hydrodehalogenation is quantified in this report on the basis of fractional dehalogenation (α_X) and benzene selectivity S_{benzene} according to

$$\alpha_x = \frac{[X]_{\text{in}} - [X]_{\text{out}}}{[X]_{\text{in}}} \quad (X = \text{Cl,Br}),$$

$$S_{\text{benzene}} = \frac{[\text{benzene}]_{\text{out}}}{[\text{haloarene}]_{\text{in}} - [\text{haloarene}]_{\text{out}}} \times 100,$$

where [ ] represents concentration and in/out refers to the inlet/outlet streams. Repeated catalytic runs with different samples from the same batch of catalyst delivered product compositions that were reproducible to within ±8%.

3. Results and discussion

3.1. Temporal hydrodehalogenation activity/selectivity

The Ni/SiO_2 catalyst promoted solely the hydrodechlorination or hydrodebromination of 1,3-DCB and 1,3-DBB, respectively, to generate partially dehalogenated CB or BB and fully dehalogenated benzene. A sequential removal of Cl from polychlorinated aromatics has been noted in a number of instances [37,38,59,60]; dehalogenation can proceed through series/parallel steps where CB or BB serves as a reactive intermediate. There was no detectable cyclohexene, cyclohexane, or cyclohexyl chloride/bromide in the product stream, i.e., 100% selectivity in terms of hydrodehalogenation. The variation of the fractional dehalogenation (α_X) of both reactants, under identical reaction conditions, with time on stream is shown in Fig. 1. Fractional dechlorination far exceeded the degree of debromination: the extracted initial debromination (see figure caption for the empirical fit to the α_X temporal response) was 0.11, considerably lower than the corresponding initial dechlorination value (0.48). Previously published kinetic analyses [61,62] revealed that variations in the gas-phase H_2 partial pressure had little effect on the dependence of reaction rate on haloarene partial pressures, an

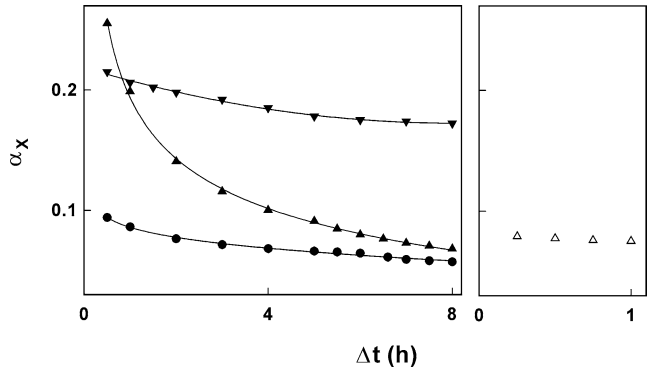

Fig. 1. Fractional hydrodehalogenation (α_x) as a function of time on stream for the conversion of 1,3-DCB (▲, freshly activated catalyst; △, after H_2 regeneration) and 1,3-DBB (●) over Ni/SiO_2 reduced at 723 K and the conversion of 1,3-DCB over Ni/SiO_2 reduced at 873 K (▼). Note: lines represent fits to $\alpha_x = (\alpha_0 \Delta t^n) \exp(-k\Delta t)$, correlation coefficients > 0.996.

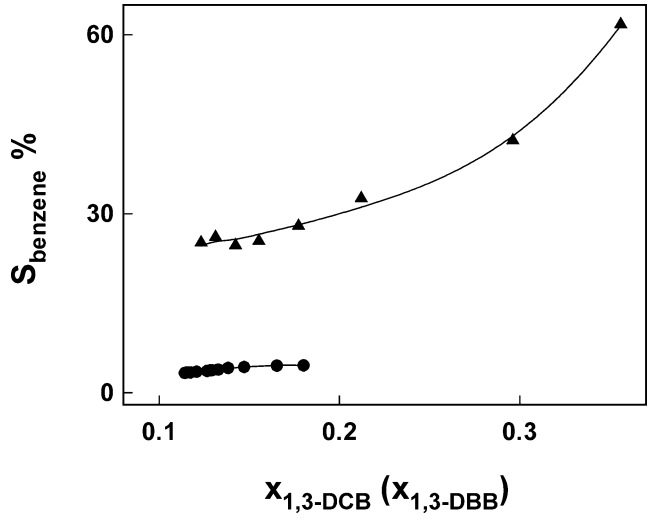

Fig. 2. Benzene selectivity (S_{benzene}) as a function of the fractional conversion of 1,3-DCB ($x_{1,3\text{-DCB}}$, ▲) and 1,3-DBB ($x_{1,3\text{-DBB}}$, ●).

effect that was taken to reflect noncompetitive adsorption of H_2 and haloarene on Ni/SiO_2. There is persuasive evidence in the literature [27,61–63] that the haloarene is adsorbed dissociatively with the formation of a surface σ-complex via the aromatic ring carbon with the highest electron density. Taking the standard physicochemical Hammet relationship as a means of estimating the electronic influence of aromatic substituents, Br has less of an inductive effect compared with Cl [64]. The electron density of the ring (C–X) carbons in DBB is accordingly lower than DCB with a resultant decrease in haloarene reactivity [63]. The difference in reactivity is immediately apparent in Fig. 2 where the fractional conversion of 1,3-DCB ($x_{1,3\text{-DCB}}$) system is markedly greater and the associated benzene selectivity is so much higher that the two sets of data are far removed with no possible overlap. The hydrodehalogenation of both 1,3-DCB and 1,3-DBB exhibited a decline with time on stream to converge at $\alpha_X < 0.05$ at $\Delta t > 8$ h. The intention of this study is to account for this loss of activity, which was not recovered

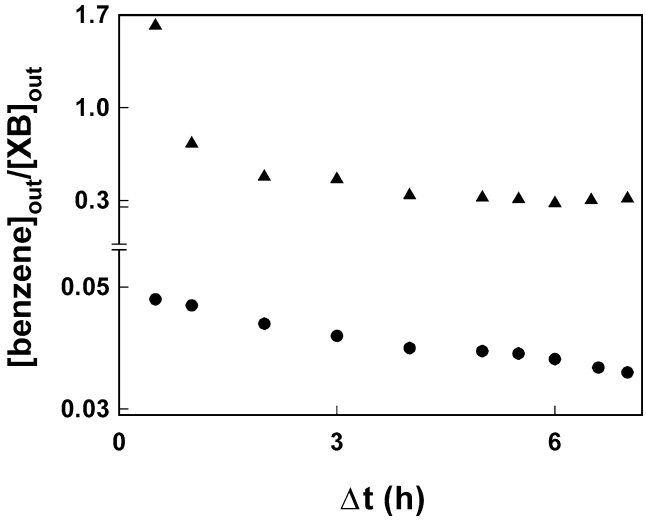

Fig. 3. Ratio of benzene to halo(Cl or Br)-benzene ($[benzene]_{out}/[XB]_{out}$) in the reactor effluent resulting from the hydrodehalogenation of 1,3-DCB (▲) and 1,3-DBB (●).

by a thermal regeneration in H_2, as is illustrated in Fig. 1 for 1,3-DCB HDC. Dehalogenation selectivity was also dependent on time on stream, as revealed in Fig. 3 in terms of the temporal response of total relative to partial hydrodehalogenation ($[benzene]_{out}/[XB]_{out}$). Loss of overall activity was accompanied by a decrease in this ratio where partial dehalogenation predominated at extended reaction times—the greater reactivity of 1,3-DCB is again in evidence.

While there was no observed benzene hydrogenation byproducts during hydrodehalogenation, the same freshly activated Ni/SiO_2 was active in the hydrogenation of benzene as feedstock: complete conversion to cyclohexane under the reaction conditions given under Section 2.7. The latter suggests quite different surface requirements for the direct hydrogenation of benzene compared with an "indirect" hydrogenation of any benzene that is generated via the hydrodehalogenation of 1,3-DCB or 1,3-DBB. It is instructive to note that Ni/SiO_2 (active for direct benzene hydrogenation), after the 8 h on stream of hydrodehalogenation (end points on Fig. 1) did not exhibit any detectable benzene hydrogenation activity on a reintroduction of the benzene feed. We have reported a similar effect for the phenol/chlorophenol reaction system [52]. While there was still residual HDC and HDB activity, contact with the haloarene served to completely inhibit benzene hydrogenation. It would appear that the catalytic deactivation induced through halogen/Ni interaction(s) exhibits some selectivity in terms of aromatic hydrogenation vs hydrogenolysis reactions.

3.2. Catalyst characterization

3.2.1. Temperature-programmed reduction

The BET surface areas of the fresh and spent catalysts are recorded in Table 1—there was no significant change in overall surface area with catalyst use. The TPR profiles generated for the direct reduction of a $NiO + SiO_2$ physical mixture (profile a) and the Ni/SiO_2 precursor (profile b) can be compared with those associated with a "rereduction" of unused (profile c) and spent (1,3-DCB: profile d, 1,3-DBB: profile e) passivated catalysts in Fig. 4. The characteristic temperatures (T_{max}) for maximum H_2 consumption are recorded in Table 1; the TPR conditions match those used for actual catalyst activation prior to hydrodehalogenation. The direct reduction of the Ni/SiO_2 generated two H_2 consumption peaks at 640 and > 700 K, which is in good agreement with previous reports of Ni/SiO_2 TPR [65–67]. The lower temperature peak has been assigned [68] to the decomposition of nickel nitrate (the precursor salt) into NiO with a subsequent reduction to Ni metal corresponding to the higher temperature peak and which matches the H_2 consumption associated with the TPR of the $NiO + SiO_2$ mix. The passivated unused sample is characterized by a single reduction peak at 540 K, diagnostic of a far more facile reduction. Vos et al. [69] and Hadjiivanov and co-workers [70] likewise observed a single low-temperature (< 500 K) peak for the reduction of passivated Ni/Al_2O_3 and Ni/SiO_2, respectively. The (passivated) Ni/SiO_2 sample (profile d) used to promote the HDC reaction exhibited similar reduction behavior to the unused (passivated) sample, albeit the T_{max} was shifted somewhat to a higher value. In contrast, reduction of the (passivated) sample after debromination was appreciably

Table 1
BET surface area, TPR H_2 consumption T_{max} values, H_2 uptakes, and TPD T_{max} values associated with the unused and spent catalysts

Catalyst	BET surface area ($m^2\,g^{-1}$)	TPR H_2 consumption T_{max} (K)[a]	H_2 uptake ($\mu mol\,g^{-1}_{catalyst}$)	H_2 TPD T_{max} (K)[a]
Ni/SiO_2, unused[b]	195	**640**, 723	43	–
Ni/SiO_2, unused[c]	190	**540**	41	560, **685**
Ni/SiO_2, unused[d]	199	**463**	17	533, **695**
$NiO + SiO_2$ physical mix, unused	185	**723**	–[e]	–[e]
Ni/SiO_2, used[c]: 1,3-DCB	202	**565**	23	570, **635**
Ni/SiO_2, used[c]: 1,3-DBB	198	**475**, 570	13	**540**

[a] Values in bold denote principal peaks.
[b] Analysis of the Ni/SiO_2 precursor ($T_{reduction} = 723$ K).
[c] Analysis of the passivated Ni/SiO_2 ($T_{reduction} = 723$ K).
[d] Analysis of the passivated Ni/SiO_2 ($T_{reduction} = 873$ K).
[e] Below detection limits.

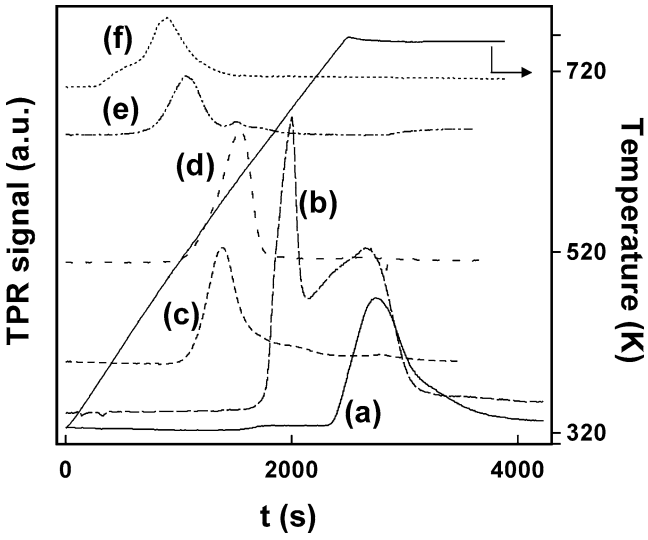

Fig. 4. TPR profiles generated for (a) $NiO + SiO_2$ physical mix, (b) Ni/SiO_2 precursor and those associated with a secondary activation of the passivated samples: (c) unused catalyst; (d) after 1,3-DCB HDC; (e) after 1,3-DBB HDB where the catalyst was reduced at 723 K; and (f) the passivated unused catalyst reduced at 873 K.

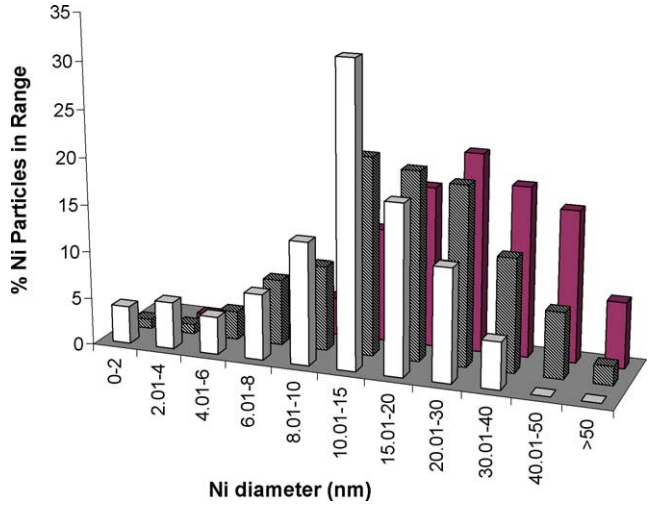

Fig. 5. Nickel particle-size distributions for the passivated Ni/SiO_2: unused (open bars); after 1,3-DCB HDC (hatched bars); (c) after 1,3-DBB HDB (solid bars).

more facile, generating a principal, though less intense, peak at ca. 475 K with a secondary higher temperature peak. Such a deviation in TPR behavior is certainly suggestive of some change to the metal phase induced during HDB that is not apparent after HDC.

3.2.2. H_2 chemisorption/TEM/XRD

The amounts of H_2 adsorbed on the unused and spent catalysts are recorded in Table 1. Hydrogen uptake on the Ni/SiO_2 precursor reduced in situ was essentially the same as that recorded after TPR of the passivated/reduced sample, indicative of an equivalency of both activation routes. The latter is significant in that it demonstrates that a characterization of the passivated samples is meaningful in terms of gaining an insight into the causes of catalyst deactivation—the controlled room temperature passivation permits storage/transfer for directly comparable ex situ analyses. The level of H_2 chemisorbed on the spent samples is significantly lower. We have avoided the assignment of metal dispersion values based on chemisorption measurements—the latter assume an exclusive H:Ni stoichiometry which is, at best, a convenient approximation and ignores the possibility of surface coverage effects and possible metal site blocking by residual halogen. Indeed, the presence of Cl is known to limit the degree of H_2 chemisorption on supported Ni [71]. Nevertheless, the lower uptake on the used catalysts can be linked to a corresponding increase of Ni particle size. Growth of Ni particles during hydrodechlorination has been noted previously [12,17,42,44]. A halide-induced agglomeration of Ni particles (on activated carbon) has been reported by Ohtsuka [72] who attributed this effect to a surface mobility of Ni–Cl species. Vaporization of $NiCl_2$ crystals at temperatures as low as 573 K has been proposed to occur, leading to a deposition and growth of surface Ni particles [73]. Chemical analysis (ICP-OES) of the activated catalysts before and after use did not reveal any significant loss of Ni from the spent samples. On the basis of the H_2 uptake values, Ni particle growth was more appreciable during the 1,3-DBB reaction. There was no detectable hydrogen uptake on bulk $NiO + SiO_2$ mixtures; any hydrogen chemisorption was below analytical detection limits.

The HRTEM-derived Ni particle-size distributions for the passivated unused and spent catalysts are given in Fig. 5. The unused sample is characterized by a rather broad distribution of Ni particle sizes that is typical of supported Ni prepared by impregnation [52]; the mean diameter is 14.0 nm. The size distributions associated with the spent samples were somewhat broader where the average Ni particle size (28.1 nm) in the sample used to convert 1,3-DBB was significantly greater than that (20.9 nm) associated with the spent catalyst from the 1,3-DCB reaction; this trend concurs with the H_2 uptake measurements. The XRD patterns for the same three samples are given in Fig. 6, where the equivalency of each is evident. The three peaks (at 44.5, 51.8, and 76.3°, corresponding to (111), (200), and (220) planes of metallic nickel) that are present in each sample are consistent with an exclusive cubic symmetry; the markers included in Fig. 6 illustrate the position and relative intensity of the XRD peaks for cubic Ni taken from the JCPDS standards [53]. Taking the signal at 44.5°, the peak width at half height, i.e., the standard peak broadening approximation, suggests an increasing average Ni particle size in the order unused < after 1,3-DCB HDC < after 1,3-DBB HDB, in accordance with the chemisorption/TEM analyses. It is instructive to note that there was no evidence whatsoever of bulk NiO; i.e., the reduction procedure was fully effective in reducing the metal component to zero valent Ni while the passivation step served to provide a protective oxide coating on the metal with no bulk NiO formation. The X-ray diffractograms also

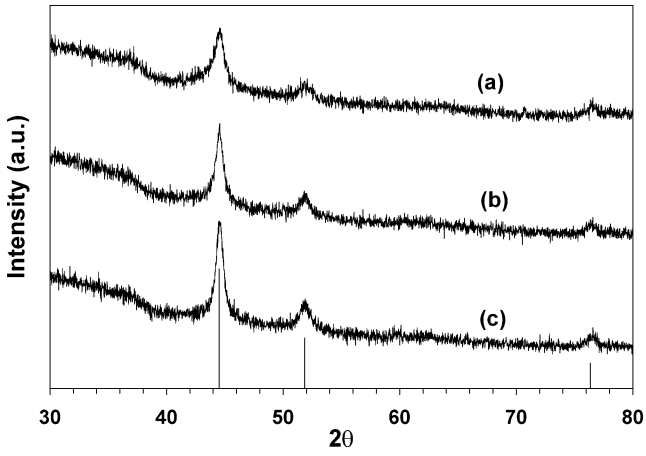

Fig. 6. XRD patterns for the passivated samples: (a) unused catalyst; (b) after 1,3-DCB HDC; (c) after 1,3-DBB HDB. Note: the solid lines indicate peak position (with relative intensity) for cubic Ni.

demonstrate a greater relative intensity of the (111) peak after catalyst use—the ratio of (111) to (200) is 3.7 for the used sample after 1,3-DBB HDB (3.5 for the used sample after 1,3-DCB HDC) compared with 2.5 for the unused sample which is in good agreement with the ratio (2.38) reported for the standard [53]. This suggests that, in addition to sintering, some restructuring of the Ni phase has taken place during hydrodehalogenation which results in a preferential development of the (111) plane. Indeed, exhaustive TEM analysis has revealed evidence of Ni particle restructuring, as can be assessed from the images provided in Fig. 7. While the supported Ni phase in the unused catalysts is characterized by essentially a spherical morphology, there is clear evidence of larger faceted Ni particles in the spent sample. There was a greater preponderance of faceted Ni in the sample used for HDB; presumably the bulkier Br induces greater change to the lattice structure. We have shown elsewhere [42] that a direct contact of Ni/SiO_2 with HX gas results in an array of particle sizes and geometrical shapes. The changes that are wrought during HDB and HDC are by no means as dramatic but particle restructuring during catalysis must be a contributing factor to the loss of activity. It should be noted that Choi and Lee [44] reported a change in metal structure from cubic to hexagonal as a result of 1,2-dichloropropane conversion over Ni/SiO_2. Moreover, they recorded an XRD peak at 15.2° that is characteristic of $NiCl_2$ and attributed its formation to HCl/Ni interactions that also resulted in the metal structural alteration. We did not observe any XRD signal due to nickel halide and can discount its presence as a bulk component in the used catalysts. However, an examination of the XRD profiles provided by Choi and Lee [44] suggests that bulk $NiCl_2$ and hexagonal Ni are not apparent at a 10% w/w Ni loading but are evident for 20 and 40% w/w Ni/SiO_2. Morato et al. [46], on the other hand, in studying the hydroconversion of CFC-12 and HFC-22 over Ni on carbonaceous supports did not observe any metal sintering but did detect (by XRD) Ni_3C formation.

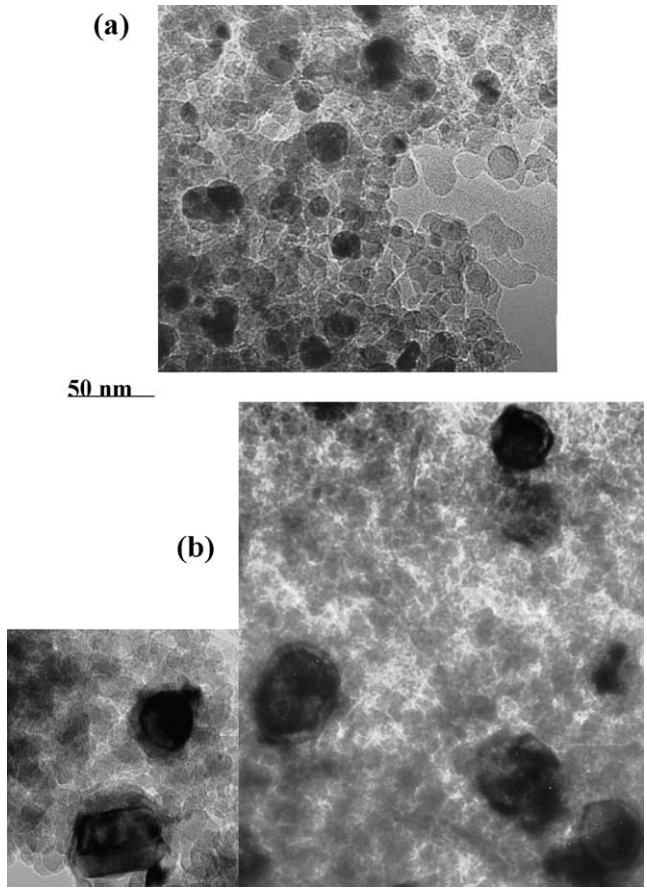

Fig. 7. TEM micrographs illustrating the morphology of the Ni crystallites on (a) unused Ni/SiO_2 and (b) Ni/SiO_2 after 1,3-DBB HDB: scale applies to all micrographs.

3.2.3. H_2 TPD

It is clear that hydrodehalogenation has led to Ni particle growth and a concomitant restructuring that resulted in a lowering of the fractional dehalogenation. While there was no evidence of bulk nickel halide formation, Cl/Br-induced changes to the Ni site electronic structure may contribute to activity loss. Temperature-programmed desorption can shed some light on changes in the electronic properties of supported metal particles [42,50]; the H_2 TPD profiles for the unused and spent samples are presented in Fig. 8. Each desorption profile is featureless at temperatures less than 450 K. The unused sample is characterized by a main desorption peak ($T_{max} = 685$ K) with a secondary lower temperature shoulder ($T_{max} = 560$ K). The sample used to promote 1,3-DCB HDC exhibits a similar two-peak response, albeit the peaks are less intense, the shoulder is ill-defined with a net shift in T_{max} of the larger peak to a lower value (see Table 1). The catalyst used in the HDB reaction shows a single less intense peak at an appreciably lower T_{max} (= 540 K). A direct comparison of the H_2 TPD profiles generated in this study with the available reports relating to Ni catalysts is problematic given the differences in metal loading/support/catalyst preparation/desorption procedure. A diversity of desorption patterns emerge with both high- (> 600 K) [31,74–76] and

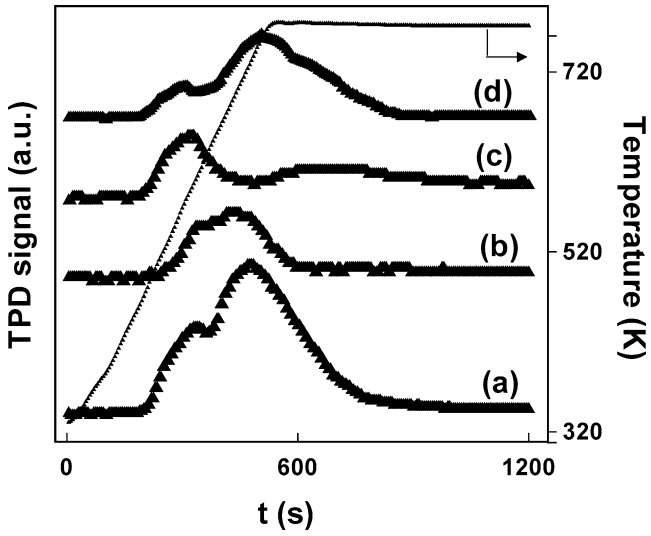

Fig. 8. H_2-TPD (to 723 K) profiles associated with the passivated Ni/SiO_2 reduced at 723 K: (a) unused; (b) after 1,3-DCB HDC; (c) after 1,3-DBB HDB; and (d) the unused passivated sample reduced at 873 K.

low-temperature peaks (< 600 K) [31,74,77] where the activation temperature [74] and nature of the cooling gas (typically H_2 or He) [78,79] have been shown to have a significant impact on the ultimate profile. We have limited the upper TPD temperature to 723 K to match the range of temperatures employed for catalyst activation and reaction. Moreover, hydrogen desorption below 650 K has been linked to hydrogen addition/scission activity of Ni catalysts [39,50, 74,80,81]. It is evident that the H_2 chemisorption/desorption behavior of Ni/SiO_2 has been disrupted due to haloarene interaction(s). The shift in T_{max} to lower values is diagnostic of weaker H/Ni interactions, indicative of some contribution due to Cl/Ni and Br/Ni contact where halogens are known to act as electron acceptors with respect to supported transition metal systems [16,82]. A visual assessment of the H_2 TPD profiles reported for fresh and used (after 1,2,4-TCB HDC) $Ni/NiAl_2O_4$ [39] also reveal a shift in the peaks (at $T < 640$ K) to lower temperatures; lower surface coverage by hydrogen for the used sample was attributed to $NiCl_2$ formation. Cesteros et al. [39] recorded HCl and Cl_2 TPD responses (at $T > 400$ K) from $Ni/NiAl_2O_4$ while Morato et al. [46] detected methane (linked to a Ni_3C phase) and HF during TPD (in H_2) of used NiAlAC. Prompted by these studies, we subjected the passivated samples to an additional high-temperature desorption with on-line mass spectroscopic analysis: the results are included in Fig. 9, wherein a small weight change ($< 3\%$) is in evidence. In the case of the unused catalyst and the HDC spent sample, this weight change is due solely to water loss associated with removal of the passivating oxide layer and desorption from the support. In the case of the HDB spent sample, there was evidence of methane generation (Fig. 9b) that can be attributed to a hydrogenation of a surface amorphous carbon species which may serve to occlude the Ni sites and contribute to catalyst deactivation/inhibition of hydrogen chemisorption.

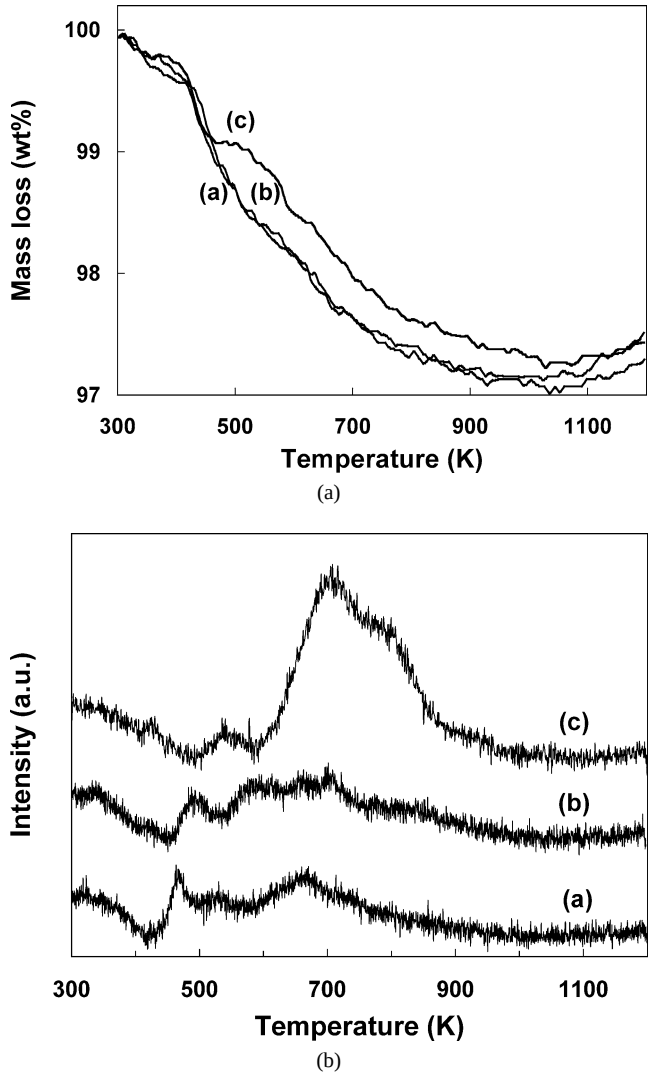

Fig. 9. (a) Mass loss (%) as a function of temperature in the hydrogen treatment (to 1173 K) of passivated samples: (a) unused catalyst; (b) after 1,3-DCB HDC; (c) after 1,3-DBB HDB. (b) Methane (mass = 16) signal intensity as a function of temperature, labeling as above.

There was, however, no evidence of any halogen release or nickel carbide formation. We have shown elsewhere [29] that the catalyst surface, under reaction conditions, is saturated with hydrogen halide. The gas sweeping of the samples that preceded passivation must have served to remove any reversibly bound residual halogen.

3.2.4. XANES/EXAFS

Extended X-ray absorption fine structure is an X-ray absorption technique, which gives detailed local structural information on the distance, number, and type of neighbors of the absorbing atom. A search through the literature has unearthed a number of reported studies of EXAFS employed in the characterization of Ni/SiO_2, principally to probe metal and metal oxide size/dispersions [83–87]. Howe et al. [88] used XANES/EXAFS to characterize the chemical state of Ni (supported on ZSM-5) before and after use in the hy-

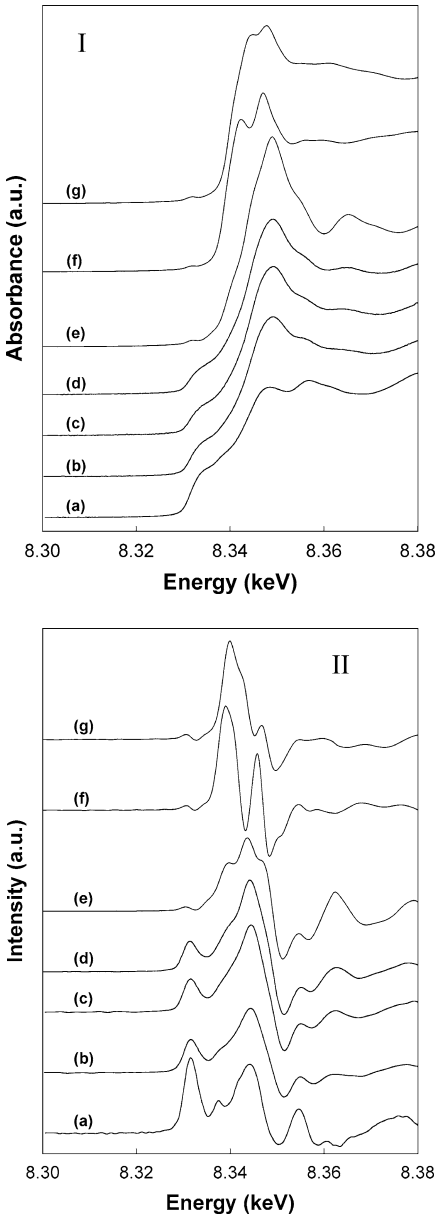

Fig. 10. Normalized Ni K edge XANES spectra (I) and XANES derivative spectra (II) of (a) Ni foil, (b) Ni/SiO_2 after 1,3-DBB HDB, (c) Ni/SiO_2 after 1,3-DCB HDC, (d) unused Ni/SiO_2, (e) $NiBr_2$, (f) $NiCl_2$, and (g) NiO.

drodehalogenation of CF_3Br and found significant differences in the Ni K edge EXAFS Fourier transforms of fresh and used catalyst, suggestive of weaker Ni–Ni interactions in the spent sample. The Ni K edge XANES spectra for the passivated unused and spent catalysts are shown in Fig. 10 which also includes the spectra of the reference materials (Ni foil, NiO, $NiCl_2$, and $NiBr_2$) for comparative purposes. It can readily be seen that there is a better match between the XANES spectra of the passivated unused/spent catalysts and the Ni foil rather than NiO. From a consideration of the derivative spectra (Fig. 10II), the metal character of the HDB spent catalyst most closely approaches that of the Ni foil. This is in keeping with the more facile TPR of the

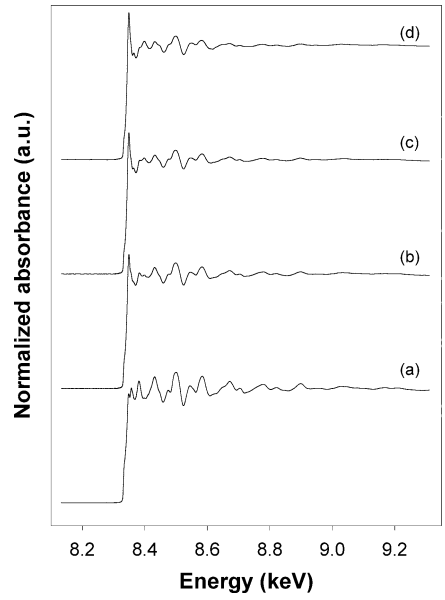

Fig. 11. Normalized EXAFS spectra measured at the Ni K edge for (a) Ni foil, (b) Ni/SiO_2 after 1,3-DBB HDB, (c) Ni/SiO_2 after 1,3-DCB HDC, and (d) unused Ni/SiO_2.

spent HDB sample, illustrated in Fig. 4. A comparison of the reference spectra for $NiCl_2$ and $NiBr_2$ with those of the used catalysts conclusively excludes the presence of any bulk nickel halide species. The background subtracted and normalized EXAFS profiles for the passivated spent/unused catalysts and the Ni foil are presented in Fig. 11. The fine structure due to "back scattering" from neighboring atoms is apparent in the oscillatory response at higher energies. The Fourier transform (FT) magnitudes of the k^0- and k^3-weighted $\chi(k)$ EXAFS functions for the same samples are depicted in Fig. 12. All the spectra exhibit an intense FT peak at ca. 2.2 Å, representing Ni atoms comprising the first coordination sphere of the central absorbing Ni. The FT peaks below 2.2 Å, for the FT based on the k^0-weighted $\chi(k)$ EXAFS function emphasizing low Z backscatterers (Fig. 12I), correspond to the presence of some oxygen atoms as is to be expected due to the presence of a passivation layer. The peak at 2.2 Å increases in intensity in the order: unused Ni/SiO_2 < Ni/SiO_2 after 1,3-DCB HDC < Ni/SiO_2 after 1,3-DBB HDB < Ni foil. The FT peaks at higher R values, corresponding to coordination shells 2, 3, and 4, also exhibit the same trend. These features are consistent with increasing metal particles size in the sequence given above. The Fourier transform magnitude in r-space and the back-Fourier transform after isolation of the first Ni–Ni metal coordination shell (k^3-weighted $\chi(k)$) are given in Fig. 13. The fitting of $\chi(k)$ was carried out in k-space and is reported as the dotted line spectra after conversion to k^3 weighting for comparison with the experimental data; the Fourier transform fitting is also displayed (dotted line). The results of the numerical simulation of the EXAFS oscillations are given in Table 2. The average value of the coordination number for the first Ni–Ni shell (N_1) associated with the unused Ni/SiO_2 is in

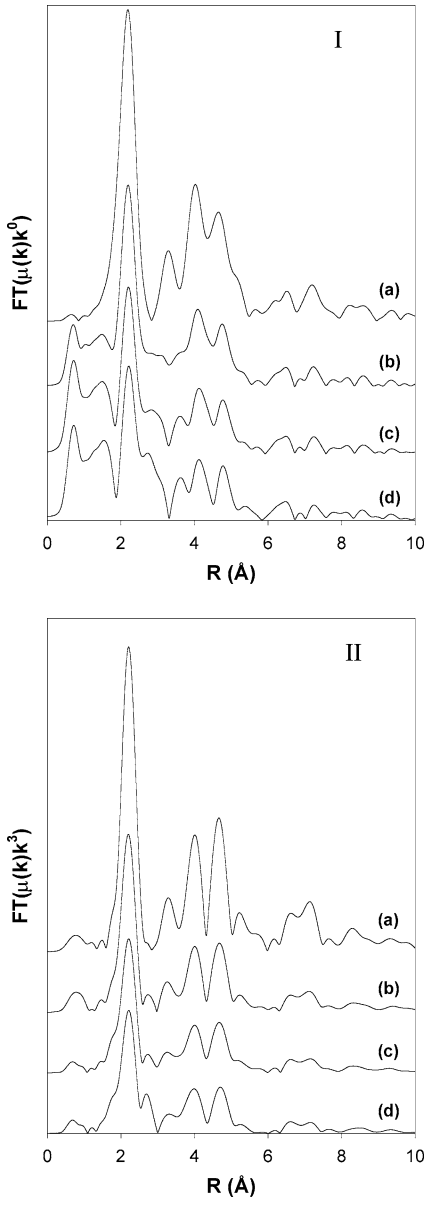

Fig. 12. k^0-weighted (I) and k^3-weighted (II) Fourier transform magnitudes of the Ni K-edge EXAFS spectra of (a) Ni foil, (b) Ni/SiO_2 after 1,3-DBB HDB, (c) Ni/SiO_2 after 1,3-DCB HDC, and (d) unused Ni/SiO_2.

good agreement with that quoted (5.8 with $S_0^2 = 0.87$) elsewhere [89] for a passivated Ni/Al_2O_3 of comparable metal loading. The order of increasing tabulated N_1 values is consistent with increasing Ni particle size and again matches the established trend.

3.3. Effect of thermal sintering of Ni on catalyst performance

The H_2 chemisorption, TEM, XRD, and EXAFS analyses of the spent deactivated samples have all revealed a Ni particle growth. In order to probe the effect of Ni size increase on hydrodehalogenation activity, the catalyst precursor was activated at the higher temperature of 873 K, in order to induce Ni sintering as noted elsewhere [68]. Indeed, the H_2 chemisorption value associated with the higher temperature reduction was markedly lower (Table 1) while TEM analyses revealed a wider distribution (< 5 to 60 nm) of particles. It is significant that the thermally sintered particles displayed a predominantly spherical morphology with no evidence of faceting. TPR of the passivated sintered catalyst (Fig. 4, profile f) is characterized by a predominant peak at 463 K, in keeping with a more facile reduction of a larger passivated Ni phase. However, the sintered Ni/SiO_2 delivered an initial HDC activity that is comparable to the catalyst activated at the lower temperature, as demonstrated in Fig. 1. Moreover, the sintered sample largely retained the HDC activity with time on stream. The observed loss of activity for the reference Ni/SiO_2 cannot then be ascribed merely to Ni agglomeration/growth as a thermal sintering of the same Ni/SiO_2 was not accompanied by a corresponding loss of HDC activity. It is instructive to note that the H_2 TPD profiles associated with unused Ni/SiO_2 reduced at both 723 and 873 K are essentially equivalent and quite distinct from those generated for the spent samples. The emergence of a low-temperature TPD shoulder in the sintered sample is, nonetheless, indicative of some commonality with the deactivated samples.

The H_2 TPD and HDC catalytic data suggest that sintering is not the intrinsic cause of the observed deactivation but is an accompanying effect. Estelle et al. [31] and Cesteros and co-workers [39] have concluded that the HDC rate is more dependent on hydrogen adsorption/desorption characteristics than on the nature of the reactive haloarene—in this study we can link Ni particle restructuring to disrupted H_2 uptake/release dynamics with a subsequent loss of dehalogenation activity. It should be noted that the TPD profiles (b) and (c) in Fig. 8 are associated with catalyst samples that exhibit residual hydrodehalogenation activities but no hydrogenation capability whatsoever: profiles (a) and (d) have been generated for catalysts that are active for both hydrodehalogenation and hydrogenation. These trends are in line with a previous study [50] where it was shown that the reactive hydrogen associated with Ni/SiO_2 that participates in hydrogen scission is quite distinct from that involved in hydrogen addition. The observed modification/faceting of the Ni particles due to Cl/Br contact is such that aromatic ring hydrogenation is completely suppressed.

4. Conclusions

Hydrodehalogenation of 1,2-DCB and 1,2-DBB over Ni/SiO_2 yields the partially dehalogenated mono-haloarene and benzene with no ring reduction. The catalyst, while highly active in the direct hydrogenation of benzene to cyclohexane, exhibits no hydrogenation activity after contact with the haloarene. Fractional dechlorination far exceeds debromination, an effect that is ascribed to the greater inductive effect of the Cl substituents that serves to activate

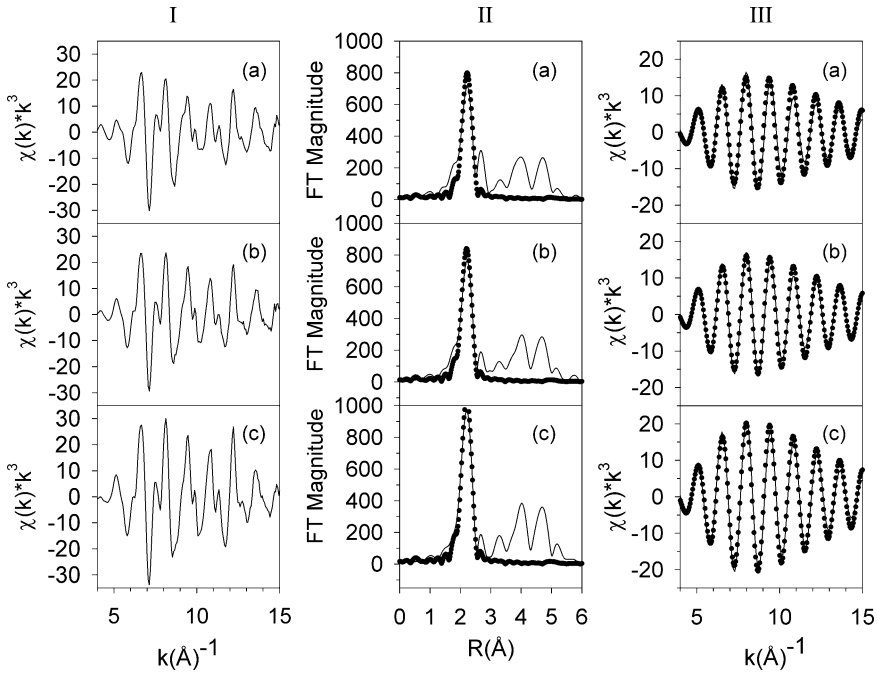

Fig. 13. EXAFS spectra for the (a) unused Ni/SiO_2, (b) Ni/SiO_2 after 1,3-DCB HDC, and (c) Ni/SiO_2 after 1,3-DBB HDB: (I) $\chi(k)k^3$ vs k; (II) the Fourier transform magnitude and (III) the Fourier-filtered inverse spectrum for the first shell, where solid lines represent experimental data and points the simulated spectrum.

Table 2
Best fit values for the average coordination number (N_1) of the first Ni–Ni shell, shift in E_0, Debye–Waller factor (σ^2), lattice expansion (delta r), and the fractional misfit (r) (relative uncertainties for these parameters are also included)

Catalyst	N_1	ΔN_1	E_0	ΔE_0	σ_2	$\Delta\sigma_2$	delta r	Δr	r factor
Ni/SiO_2, unused	5.58	0.42	7.9	0.80	0.0034	0.0008	−0.0071	0.0061	0.0426
Ni/SiO_2, used: 1,3-DCB	6.17	0.32	6.6	0.56	0.0037	0.0005	−0.0056	0.0043	0.0200
$NiSiO_2$, used: 1,3-DBB	7.72	0.51	6.6	0.71	0.0037	0.0007	−0.0035	0.0054	0.0320
Ni foil	12.00								
$S_0^2 = 0.8652$									

the ring for hydrogenolytic attack. Ni/SiO_2 was subject to a temporal loss of activity that was accompanied by Ni particle growth and structural modification with a consequent disruption to the hydrogen adsorption/desorption surface dynamics. Nickel growth during HDC and HDB has been established by TPR, H_2 chemisorption, TEM, XRD, and EXAFS. The XRD analyses did not reveal any bulk nickel halide formation and no halide species were detected in the effluent gases during TPR/MS analysis of the spent samples. While the Ni complement in both unused and used catalysts exhibits an exclusive cubic symmetry, the used catalysts demonstrated a greater preference for the (111) orientation than was prevalent before use and Cl/Br contact resulted in appreciable Ni particle faceting. Nickel sintering was independently induced by thermal means where the resultant sintered catalyst delivered comparable hydrodehalogenation activities, Ni morphology, and H_2 TPD behavior. We propose that the predominant cause of deactivation is a haloarene or halide-induced irreversible alteration to the Ni site structure.

Acknowledgments

This work was supported in part by the National Science Foundation through Grant CTS-0218591 and the Commonwealth of Kentucky. EXAFS/XANES measurements were conducted at the National Synchrotron Light Source (Beamline X18B), Brookhaven National Laboratory, supported by the US DOE, Division of Materials and Chemical Sciences.

References

[1] A.A. Meharg, J. Wright, D. Obson, Sci. Total Environ. 251–252 (2000) 243.
[2] A. Miyazaki, T. Amano, S.H. Hotaka, Y. Nakano, Chemosphere 47 (2002) 65.
[3] M.-J. Wang, S.P. Mc Grath, K.C. Jones, Sci. Total Environ. 121 (1992) 159.
[4] D.T. Allen, in: A.E. Martell, D. Sawyer (Eds.), Industrial Environmental Chemistry: Waste Minimization in Industrial Processes and Remediation of Hazardous Wastes, Plenum, New York, 1992, p. 89.
[5] E.D. Goldberg, Sci. Total Environ. 100 (1991) 17.

[6] C. Denbesten, J.J.R.M. Vet, H.T. Besselink, G.S. Kiel, B.J.M. Vanberkel, R. Beems, P.J. Vandladeren, Toxicol. Appl. Pharm. 11 (1991) 69.
[7] US Environmental Protection Agency, Report 40, Part 122, US Gov. Printing Office, Washington, DC, 1998.
[8] K. Tuppuraien, I. Halonen, P. Ruokojarvi, J. Tarhanen, J. Ruusknen, Chemosphere 36 (1998) 1493.
[9] D.R. van der Vaart, E.G. Marchand, A. Bagely-Pride, Crit. Rev. Environ. Sci. Technol. 24 (1994) 203.
[10] A. Converti, M. Zilli, D.M. De Faveri, G. Ferraiolo, J. Hazard. Mater. 27 (1991) 127.
[11] B.F. Hagh, D.T. Allen, Innovative Hazardous Waste Treatment Technology, TECHNOMIC, Freemont, Lancaster, PA, 1990.
[12] M.A. Keane, in: M.A. Keane (Ed.), Interfacial Applications in Environmental Engineering, Dekker, New York, 2002, p. 231.
[13] M.K. Cieplik, O.J. Epema, R. Louw, Eur. J. Org. Chem. (2002) 2792.
[14] A.H. Weiss, S. Valinski, G.V. Antoshin, J. Catal. 74 (1982) 136.
[15] K.A. Frankel, B.W.L. Jang, G.W. Roberts, J.J. Spivey, Appl. Catal. A 209 (2001) 401.
[16] B. Coq, G. Ferrat, F. Figueras, J. Catal. 101 (1986) 434.
[17] A. Gampine, D. Eyeman, J. Catal. 179 (1998) 315.
[18] J.W. Bozelli, Y.M. Chen, S.S.C. Chuang, Chem. Eng. Commun. 115 (1992) 1.
[19] M. Kraus, V. Bazant, in: J.W. Hightower (Ed.), Proceedings of the 5th International Congress on Catalysis, North-Holland, New York, 1973, p. 1073.
[20] E.J. Creyghton, M.H.W. Burgers, J.C. Jensen, H. van Bekkum, Appl. Catal. A 128 (1995) 275.
[21] Y. Cesteros, P. Salagre, F. Medina, J.E. Sueiras, Appl. Catal. B 25 (2000) 213.
[22] M.A. Aramendia, V. Boráu, I.M. Garcia, J.M. Jiménez, J.M. Marinas, F.J. Urbano, Appl. Catal. B 20 (1999) 101.
[23] L. Prati, M. Rossi, Appl. Catal. B 23 (1999) 135.
[24] A.Y. Stakheev, L.M. Kustov, Appl. Catal. A 188 (1999) 3.
[25] F.J. Urbano, J.M. Marinas, J. Mol. Catal. A: Chem. 173 (2001) 329.
[26] B. Coq, F. Figueras, S. Hub, D. Tournigant, J. Phys. Chem. 99 (1995) 11159.
[27] B.F. Hagh, D.T. Allen, Chem. Eng. Sci. 45 (1990) 2695.
[28] G. Tavoularis, M.A. Keane, J. Mol. Catal. A: Chem. 142 (1999) 187.
[29] G. Tavoularis, M.A. Keane, J. Chem. Technol. Biotechnol. 74 (1999) 60.
[30] G. Tavoularis, M.A. Keane, Appl. Catal. A 182 (1999) 309.
[31] J. Estelle, J. Ruz, Y. Cesteros, R. Fernandez, P. Salagre, F. Medina, J.-E. Sueiras, J. Chem. Soc., Faraday Trans. 92 (1996) 2811.
[32] A.R. Suzdorf, S.V. Morozov, N.N. Anshits, S.I. Tsiganova, A.G. Anshits, Catal. Lett. 29 (1994) 49.
[33] B.F. Hagh, D.T. Allen, AIChE J. 36 (1990) 773.
[34] J. Frimmel, M. Zdražil, J. Catal. 167 (1997) 286.
[35] D.I. Kim, D.T. Allen, Ind. Eng. Chem. Res. 36 (1997) 3019.
[36] N. Lingaiah, Md.A. Uddin, A. Muto, T. Iwamoto, Y. Sakata, Y. Kusano, J. Mol. Catal. A: Chem. 161 (2000) 157.
[37] E.J. Shin, M.A. Keane, Chem. Eng. Sci. 54 (1999) 1109.
[38] E.J. Shin, M.A. Keane, J. Chem. Technol. Biotechnol. 75 (2000) 159.
[39] Y. Cesteros, P. Salagre, F. Medina, J.E. Sueiras, Catal. Lett. 67 (2000) 147.
[40] Z. Yu, S. Liao, Y. Xu, React. Funct. Polym. 29 (1996) 151.
[41] B. Wei, S. Li, H.K. Lee, T.S.A. Hor, J. Mol. Catal. A: Chem. 126 (1997) 183.
[42] C. Park, C. Minini, J.L. Valverde, M.A. Keane, J. Catal. 211 (2002) 451.
[43] R.J. Meyer, I. Kim, D.T. Allen, J.H. Jo, Chem. Eng. Sci. 54 (1999) 3627.
[44] Y. Choi, W.Y. Lee, Catal. Lett. 67 (2000) 155.
[45] M. Martino, R. Rosal, H. Sastre, F.V. Diez, Appl. Catal. B 20 (1999) 301.
[46] A. Morato, C. Alonso, F. Medina, P. Salagre, J.E. Sueiras, R. Terrado, A. Giralt, Appl. Catal. B 23 (1999) 175.
[47] Y. Cesteros, P. Salagre, F. Medina, J.E. Sueiras, D. Tichit, B. Coq, Appl. Catal. B 32 (2001) 25.
[48] Y. Cesteros, P. Salagre, F. Medina, J.E. Sueiras, Appl. Catal. B 22 (1999) 135.
[49] C. Menini, C. Park, E.-J. Shin, G. Tavoularis, M.A. Keane, Catal. Today 62 (2000) 355.
[50] E.-J. Shin, A. Spiller, G. Tavoularis, M.A. Keane, Phys. Chem. Chem. Phys. 1 (1999) 3173.
[51] M.A. Keane, G. Tavoularis, React. Kinet. Catal. Lett. 78 (2003) 11.
[52] G. Pina, C. Louis, M.A. Keane, Phys. Chem. Chem. Phys. 5 (2003) 1924.
[53] JCPDS-ICDD, PCPDFWIN, Version 2.2, June 2001.
[54] T. Ressler, J. Synchrotron Radiat. 5 (1998) 118.
[55] T. Ressler, J. Phys. IV 7 (1997) C2-269.
[56] M. Newville, B. Ravel, D. Haskel, J.J. Rehr, E.A. Stern, Y. Yacoby, Phys. B 208 (1995) 154.
[57] J.J. Rehr, R.C. Albers, S.I. Zabrinsky, Phys. Rev. Lett. 69 (1992) 3397.
[58] B. Ravel, J. Synchrotron Radiat. 8 (2001) 314.
[59] F. Murena, V. Famiglietti, F. Gioia, Environ. Prog. 12 (1993) 233.
[60] V.A. Yakovlev, V.V. Terskikh, V.I. Simagina, V.A. Likholobov, J. Mol. Catal. A: Chem. 153 (2000) 231.
[61] M.A. Keane, D.Yu. Murzin, in: D.G. Morrell (Ed.), Catalysis of Organic Reactions, Dekker, New York, 2002, p. 595.
[62] M.A. Keane, D.Yu. Murzin, Chem. Eng. Sci. 56 (2001) 3185.
[63] Yu.A. Serguchev, Yu.V. Belokopytov, Kinet. Catal. 42 (2001) 174.
[64] J.A. Dean, Handbook of Organic Chemistry, McGraw–Hill, New York, 1987.
[65] T. Mizushima, K. Nishida, H. Ohkita, N. Kakuta, Bull. Chem. Soc. Jpn. 75 (2002) 2283.
[66] J. Zielinski, Catal. Lett. 31 (1995) 47.
[67] M.A. Keane, Can. J. Chem. 72 (1994) 372.
[68] C. Louis, Z.X. Cheng, M. Che, J. Phys. Chem. 97 (1993) 5703.
[69] B. Vos, E. Poels, A. Bliek, J. Catal. 198 (2001) 77.
[70] K. Hadjiivanov, M. Mihaylov, D. Klissurski, P. Stefanov, N. Abadjieva, E. Vassileva, L. Mintchev, J. Catal. 185 (1999) 314.
[71] D.J. Moon, M.J. Chung, K.Y. Park, S.I. Hong, Appl. Catal. A 168 (1998) 159.
[72] Y. Ohtsuka, J. Mol. Catal. 54 (1989) 225.
[73] C. Hoang-Van, Y. Kachaya, S.J. Teichner, J. Phys. Chem. B 101 (1997) 7060.
[74] S. Smeds, T. Salmi, L.P. Lindfors, O. Krause, Appl. Catal. A 144 (1996) 177.
[75] G.D. Weatherbee, C.H. Bartholomew, J. Catal. 87 (1984) 55.
[76] R. Kramer, M. Andre, J. Catal. 58 (1979) 287.
[77] J.A. Konvalinka, P.H. van Oeffelt, J.J.F. Scholten, Appl. Catal. 1 (1981) 141.
[78] P.I. Lee, Y.J. Huang, J.C. Heydweiller, J.A. Schwartz, Chem. Eng. Commun. 63 (1989) 205.
[79] D.W. Stockwell, G. Bertucco, G.W. Coulston, C.O. Bennett, J. Catal. 113 (1988) 317.
[80] E.-J. Shin, M.A. Keane, Ind. Eng. Chem. Res. 39 (2000) 883.
[81] P. Marecot, E. Paraiso, J.M. Dumas, J. Barbier, Appl. Catal. 74 (1991) 261.
[82] T. Halchev, E. Ruckenstein, J. Catal. 73 (1982) 171.
[83] J.P. Espinos, A.R.G. Elipe, A. Caballero, J. Garcia, G. Munuera, J. Catal. 136 (1992) 415.
[84] W.B. Ding, W. Tuntawiroon, J. Liang, L.L. Anderson, Fuel Process. Technol. 49 (1996) 49.
[85] J.C. Yang, Y.G. Shul, M. Che, Catal. Today 44 (1998) 315.
[86] S. Takenaka, H. Ogihara, K. Otsuka, J. Catal. 208 (2002) 54.
[87] C. Louis, Z.X. Cheng, M. Che, J. Phys. Chem. 97 (1993) 5703.
[88] R.F. Howe, S. Thomson, Y. Yang, K. Lee, E.M. Kennedy, B.Z. Dlugogorski, J. Mol. Catal. A: Chem. 181 (2002) 63.
[89] T. Shido, M. Lok, R. Prins, Top. Catal. 8 (1999) 223.